

Problem 1

- (a) *Proof.* Let λ be an eigenvalue of A s.t. $Au = \lambda u$, $u \neq 0$. By the self-adjointness of A , we have

$$\lambda \|u\|^2 = \langle \lambda u, u \rangle = \langle Au, u \rangle = \langle u, Au \rangle = \langle u, \lambda u \rangle = \bar{\lambda} \|u\|^2.$$

Since $\|u\|^2 \neq 0$, $\lambda = \bar{\lambda}$, which implies $\lambda \in \mathbb{R}$. □

- (b) *Proof.* Suppose $Ae_i = \lambda_i e_i$, $Ae_j = \lambda_j e_j$ with $\lambda_i \neq \lambda_j$. By the self-adjointness of A , we have

$$\lambda_i \langle e_i, e_j \rangle = \langle \lambda_i e_i, e_j \rangle = \langle Ae_i, e_j \rangle = \langle e_i, Ae_j \rangle = \langle e_i, \lambda_j e_j \rangle = \bar{\lambda}_j \langle e_i, e_j \rangle.$$

Since $\lambda_i \neq \bar{\lambda}_j = \lambda_j$, $\langle e_i, e_j \rangle = 0$, which implies that e_i, e_j are orthogonal. □

Problem 2

We implement SMACOF (Figure 1b) and isomap (Figure 1c, 1d). As we see from the results, SMACOF preserves the Euclidean distance in \mathbb{R}^3 , while isomap recovers the geodesic distance on the 2D manifold (Figure 1d). However, isomap is highly sensitive to the choice of parameters, and is very likely to fail, since bad parameters may lead to shortcuts between non-intersecting neighbourhoods (in Figure 1c, a shortcut stitches two parts of the Swiss roll together, making the band into a loop in \mathbb{R}^2).

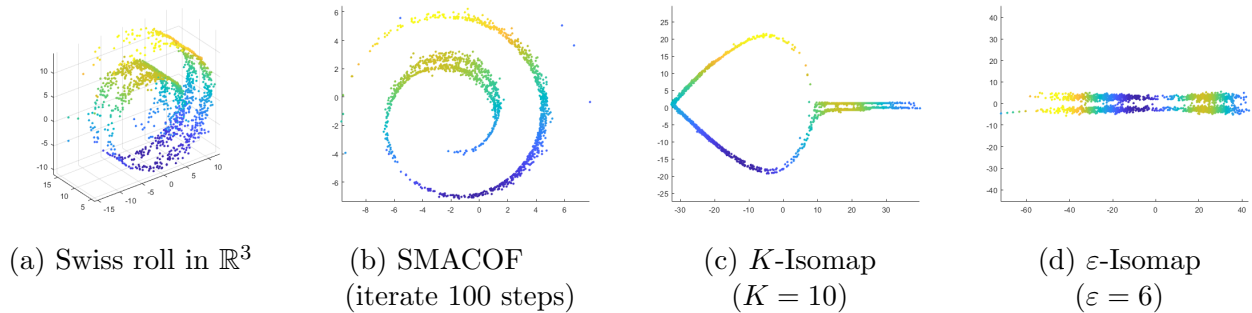


Figure 1: Embed a point cloud in \mathbb{R}^3 with two-dimensional structure into \mathbb{R}^2 .

Problem 3

- (a) The eigenfunctions of the Laplacian-Beltrami operator for the smallest 10 eigenvalues are shown in Figure 2. As the eigenvalues getting larger, the approximation for the eigenfunctions becomes inaccurate (Figure 3).

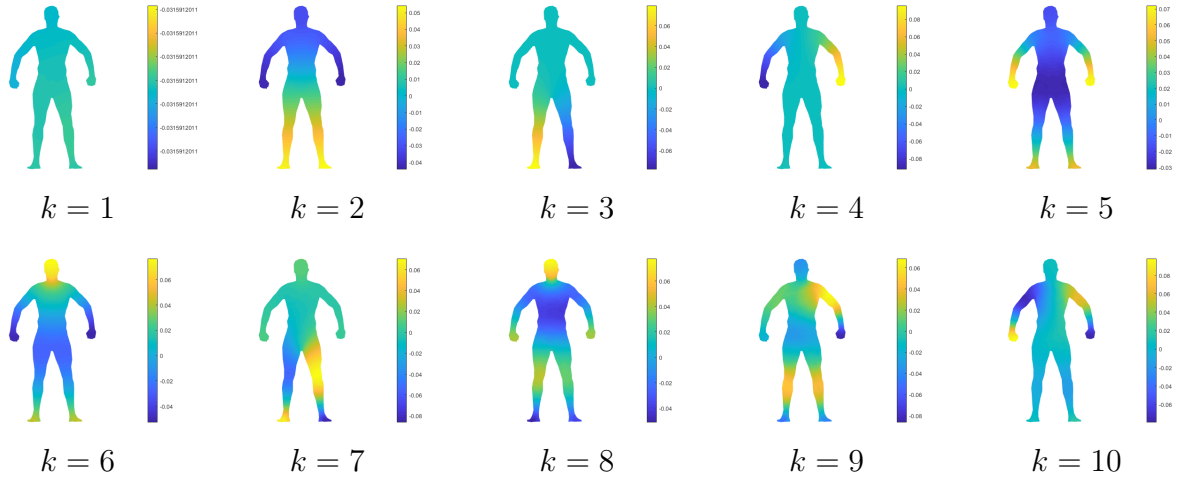


Figure 2: Eigenfunctions of the Laplacian-Beltrami operator for the smallest 10 eigenvalues.

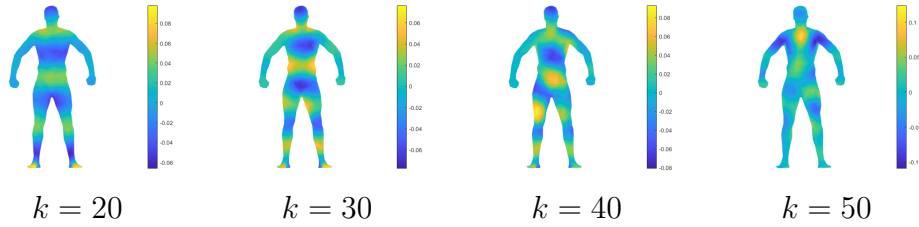


Figure 3: Eigenfunctions of the Laplacian-Beltrami operator for large eigenvalues.

- (b) The scaled heat kernel signatures with $k = 300, n = 500$ is shown in Figure 4b.
- (c) The scaled heat kernel signatures with different number of eigenfunctions and different number of samples for approximation are shown in Figure 4. As the number of eigenfunctions grows, the plot of HKS shifts right and more features of the function are revealed (see Figure 4a, 4b, 4c). As the number of samples grows, we get a denser sampled plot of the same shape (see Figure 4d, 4b).
- (d) The differences of HKS's w.r.t. given fixed points are shown in Figure 5. From the results we see that the HKS is discriminative between points with different neighbourhood structures (Figure 5a, 5b and Figure 5c, 5d); however, it is not good at distinguishing between points with similar neighbourhoods, especially when strong symmetry exists.

Problem 4

Proof. Let Σ be a surface in \mathbb{R}^3 with boundary, let g be the metric on Σ and $\varphi : \mathbb{R}^2 \supset \Omega \rightarrow \Sigma$ be a parameterization of Σ . First we show that for a vector field V on Σ ,

$$\operatorname{div} V := \nabla_{\frac{\partial}{\partial x^i}} V^i = \frac{\partial V^i}{\partial x^i} + \Gamma_{ij}^i V^j = \frac{1}{\sqrt{\det(g)}} \frac{\partial}{\partial x^i} \left(\sqrt{\det(g)} V^i \right).$$

By product rule and Jacobi's formula for derivative of determinants,

$$\begin{aligned} \frac{1}{\sqrt{\det(g)}} \frac{\partial}{\partial x^i} \left(\sqrt{\det(g)} V^i \right) &= \frac{1}{\sqrt{\det(g)}} \left(\frac{(\det(g))_i}{2\sqrt{\det(g)}} V^i + \sqrt{\det(g)} \frac{\partial V^i}{\partial x^i} \right) \\ &= \frac{\partial V^i}{\partial x^i} + \frac{1}{2\det(g)} (\det(g))_i V^i \\ &= \frac{\partial V^i}{\partial x^i} + \frac{1}{2} g^{kl} g_{kl,i} V^i. \end{aligned}$$

Since

$$\begin{aligned} g_{kl,i} &= \frac{\partial}{\partial x^i} \left\langle \frac{\partial}{\partial x^k}, \frac{\partial}{\partial x^l} \right\rangle = \left\langle \nabla_{\frac{\partial}{\partial x^i}} \frac{\partial}{\partial x^k}, \frac{\partial}{\partial x^l} \right\rangle + \left\langle \frac{\partial}{\partial x^k}, \nabla_{\frac{\partial}{\partial x^i}} \frac{\partial}{\partial x^l} \right\rangle \\ &= \left\langle \Gamma_{ik}^p \frac{\partial}{\partial x^p}, \frac{\partial}{\partial x^l} \right\rangle + \left\langle \frac{\partial}{\partial x^k}, \Gamma_{il}^q \frac{\partial}{\partial x^q} \right\rangle = \Gamma_{ik}^p g_{pl} + \Gamma_{il}^q g_{qk}, \end{aligned}$$

we have

$$\begin{aligned} \frac{1}{\sqrt{\det(g)}} \frac{\partial}{\partial x^i} \left(\sqrt{\det(g)} V^i \right) &= \frac{\partial V^i}{\partial x^i} + \frac{1}{2} g^{kl} (\Gamma_{ik}^p g_{pl} + \Gamma_{il}^q g_{qk}) V^i \\ &= \frac{\partial V^i}{\partial x^i} + \frac{1}{2} (\Gamma_{ik}^p \delta_{pk} + \Gamma_{il}^q \delta_{ql}) V^i = \frac{\partial V^i}{\partial x^i} + \frac{1}{2} (\Gamma_{ik}^k + \Gamma_{il}^l) V^i \\ &= \frac{\partial V^i}{\partial x^i} + \Gamma_{ij}^j V^i = \operatorname{div} V. \end{aligned}$$

Finally, using the divergence theorem on \mathbb{R}^2 , we have

$$\begin{aligned} \int_{\Sigma} \operatorname{div} V \, d\sigma &= \int_{\Sigma} \frac{1}{\sqrt{\det(g)}} \frac{\partial}{\partial x^i} \left(\sqrt{\det(g)} V^i \right) d\sigma = \int_{\Omega} \frac{\partial}{\partial x^i} \left(\sqrt{\det(g)} V^i \right) dx^1 dx^2 \\ &= \int_{\partial\Omega} \sqrt{\det(g)} \langle V, \mathbf{n}_0 \rangle dl = \int_{\partial\Sigma} \langle V, \mathbf{n} \rangle ds \end{aligned}$$

where \mathbf{n}_0 is the outward normal of $\partial\Omega$, \mathbf{n} is the outward normal of $\partial\Sigma$, l, s are the Hausdorff measures on $\partial\Omega, \partial\Sigma$ respectively. This completes the proof. \square

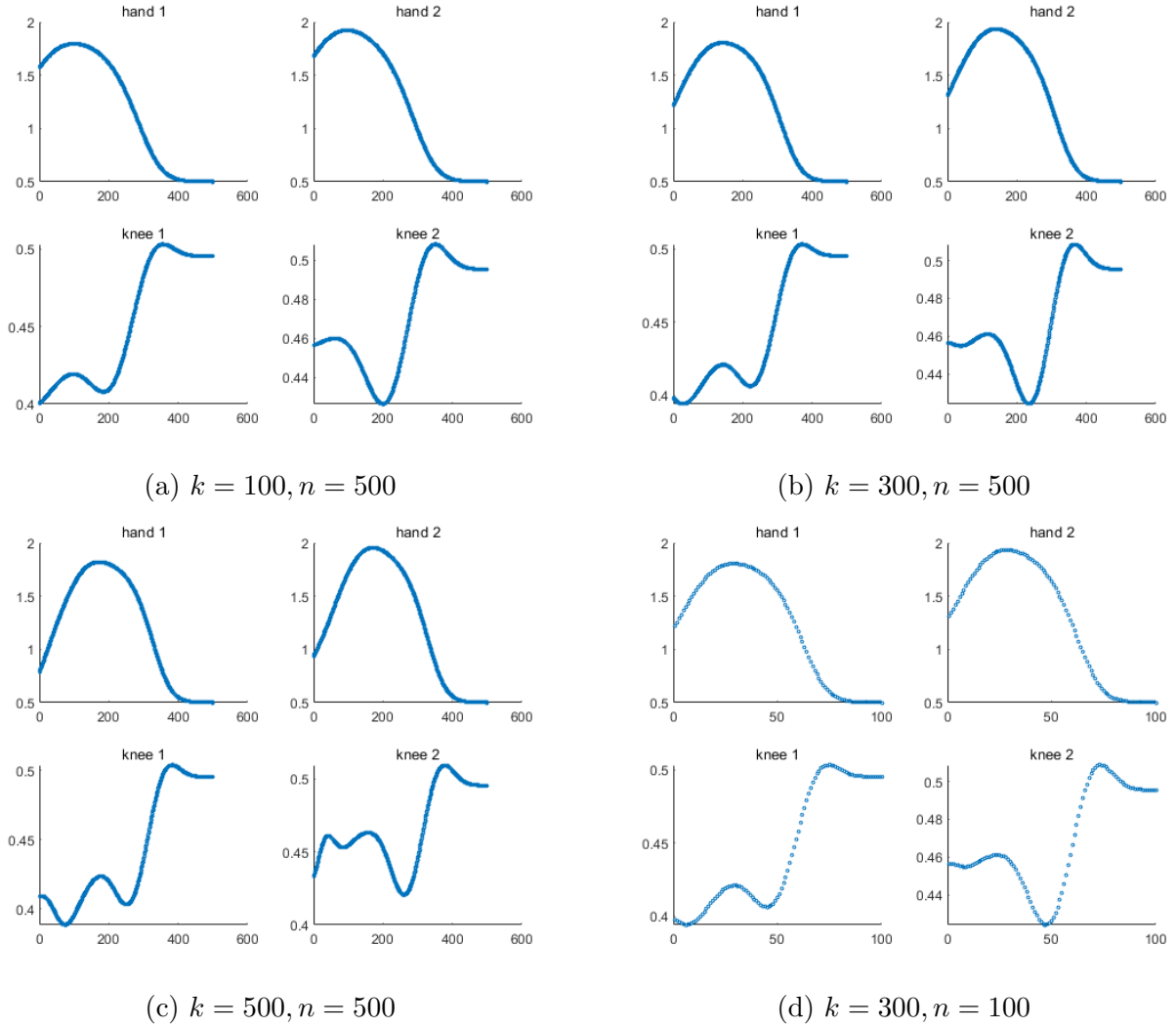


Figure 4: Heat kernel signatures of the two hands and two knees.

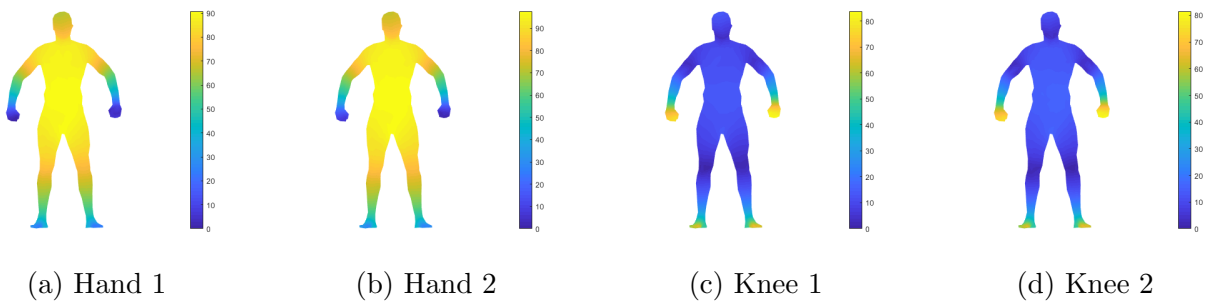


Figure 5: Differences of heat kernel signatures w.r.t. a fixed point.